Available online at www.sciencedirect.com
ScienceDirect
Journal of Sound and Vibration 306 (2007) 238–251
JOURNAL OF SOUND AND VIBRATION
www.elsevier.com/locate/jsvi

Impact damper for controlling friction-driven oscillations

P.B. Zinjade, A.K. Mallik*

Department of Mechanical Engineering, Indian Institute of Technology, Kanpur 208016, India

Received 28 June 2006; received in revised form 5 May 2007; accepted 12 May 2007
Available online 5 July 2007

Abstract

Control of friction-driven oscillations by using an impact damper is investigated. An experimental setup of a single degree-of-freedom friction-driven oscillator with an attached impact damper is designed and fabricated. An approximate nonlinear mathematical model of the friction-driven oscillator is derived. The values of unknown parameters in this mathematical model are obtained by using a least square error method so as to match the experimentally obtained response. An approximate solution of the general steady-state response of the friction-driven oscillator with an attached impact damper is derived analytically by using a piecewise equivalent linearization approach assuming two non-symmetric impacts per cycle. The effects of mass ratio, coefficient of restitution and clearance on the performance of the impact damper have been investigated analytically and the results are verified by numerical integration. Experimental results obtained for steel-on-steel, aluminum-on-aluminum and aluminum-on-rubber impacts are reported.

1. Introduction

Friction-driven oscillation is a kind of self-excited vibration in which the variable friction force generates a periodic motion. The characteristics of the friction force are quite complex and depend on the normal pressure, slip velocity, surface and material properties [1]. The friction-actuated oscillation is a strongly nonlinear, discontinuous and non-smooth process, which is a source of instabilities generating stick–slip, chatter, squeal, and chaos [2,3]. One of the most significant causes of the friction-induced instabilities is the negative gradient (i.e., negative damping) characteristic of the friction force with respect to the slip velocity [4]. The energy needed for the oscillations to grow is provided by this friction force until this negative damping effect is restrained by some nonlinear effect which leads to a periodic solution i.e., a steady-state limit cycle. Generally in a nonlinear friction model, the friction force appears as a function of slip velocity up to cubic order [5,6].

Various active and passive methods of controlling the friction-driven oscillation have been investigated. One of the passive control methods is the use of an impact damper in which repeated impacts are used to control the vibration. Easy design and constructional features of an impact damper have attracted many of the researchers to develop an efficient methodology for studying its performance [7]. An idealized model of an impact damper consists of a secondary loose mass undergoing repeated collisions with the primary vibratory

*Corresponding author.
E-mail address: akmallik@iitk.ac.in (A.K. Mallik).

0022-460X/$ - see front matter © 2007 Elsevier Ltd. All rights reserved.
doi:10.1016/j.jsv.2007.05.017

system [8]. Both the transfer of momentum to the secondary mass and the dissipation of energy at the time of impact control the vibration of the primary system. The performance of an impact damper depends on various system parameters such as mass ratio, coefficient of restitution and clearance [9]. The general motion of an impact damper is a nonlinear and discontinuous process. The clearance and impact nonlinearity in an impact damper is easy to generate and control. It has also been reported that a suitable use of nonlinear vibration neutralizer is more effective than a linear vibration neutralizer. Hence, the impact damper operates more effectively than the classical dynamic vibration damper [10,11]. Analytical and experimental studies have demonstrated that a class of nonlinear auxiliary mass damper can be effectively used to neutralize the vibrations of various systems like turbine blades, long and thin cutting tools like drills or boring tools [12–14].

Generally two symmetric impacts per cycle of the primary system have been considered to derive the general motion of an impact damper. Chatterjee et al. [15,16] used a piecewise equivalent linearization approach to derive a general motion of nonlinear systems with two symmetric impacts per cycle. But Masri [17] assumed two non-symmetric impacts per cycle for obtaining analytical solution of the general steady-state response of a harmonically excited primary system provided with an impact damper. Recently impact dampers have also been used to control chaotic motion [18].

In the present work, the standard spring-mass system having a single degree-of-freedom and placed on a belt moving at a constant speed is considered as an idealized experimental model for the friction-driven oscillator. Under pure slip condition, the friction force is represented by Taylor's series expansion up to three terms to derive an approximate mathematical model. The unknown coefficients of the linear, square and cubic terms of the Taylor's series are obtained so as to match the experimentally obtained response. For this numerical analysis, a least square error method and backward difference approach with 4096 data points is used. The performance of the impact damper is studied analytically by using the piecewise equivalent linearization method with two non-symmetric impacts per cycle. The analytical results are compared with that obtained from direct numerical integration of the equations of motion. The effects of various system parameters like the coefficient of restitution, clearance and the mass ratio are discussed. Experiments are conducted for steel–steel, aluminum–aluminum and aluminum–rubber impacts. The values of coefficients of restitution for some of these impacts are obtained approximately from the graphs given in Ref. [19].

2. Friction-driven oscillator

2.1. Mathematical model

Fig. 1 shows the standard mass on a moving belt model of a friction oscillator. From the experimental results (to be presented in a subsequent section), it was confirmed that the pure slip oscillations without any sticking occur, i.e., the velocity of the mass $\dot{X}(t) < V_0$ for all values of t at steady state, where V_0 is the constant belt speed and t denotes time with X as indicated in the figure. Thus, the condition of pure slip is satisfied.

The equation of the motion of the mass can be written as

$$M\ddot{X}(t) + kX(t) = F(V_0 - \dot{X}(t)) \text{ as } \dot{X}(t) < V_0, \tag{1}$$

where F is the friction force and k the linear spring stiffness.

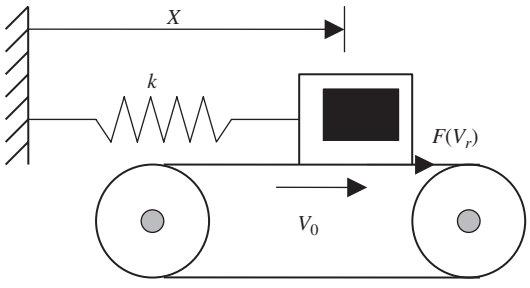

Fig. 1. Mass on a moving belt system.

It is convenient to introduce a new variable $x(t)$, replacing $X(t)$ as

$$x(t) = X(t) - \frac{F(V_0)}{k}. \tag{2}$$

Therefore, Eq. (1) becomes

$$M\ddot{x}(t) + kx(t) = F(V_0 - \dot{x}(t)) - F(V_0). \tag{3}$$

It is assumed that the frictional force can be adequately expressed as a Taylor's series up to three terms in the range of $V_r = V_0 - \dot{x}(t)$ ($V_0 > \dot{x}(t)$, so V_r is always positive). Assuming $\dot{x}(t)$ to be small and the Taylor's series converges rapidly enough to justify the use of only first three terms, we have

$$\begin{aligned} F(V_0 - \dot{x}(t)) - F(V_0) &= F(V_0) - \left.\frac{\mathrm{d}F}{\mathrm{d}V}\right|_{V=V_0} \dot{x}(t) + \frac{1}{2!}\left.\frac{\mathrm{d}^2F}{\mathrm{d}V^2}\right|_{V=V_0} \dot{x}^2(t) - \frac{1}{3!}\left.\frac{\mathrm{d}^3F}{\mathrm{d}V^3}\right|_{V=V_0} \dot{x}^3(t) - F(V_0) \\ &= -F_V^{(1)}\dot{x}(t) + \frac{F_V^{(2)}}{2}\dot{x}^2(t) - \frac{F_V^{(3)}}{6}\dot{x}^3(t), \end{aligned} \tag{4}$$

where

$$F_V^{(1)} = \left.\frac{\mathrm{d}F}{\mathrm{d}V}\right|_{V=V_0}; \quad F_V^{(2)} = \left.\frac{\mathrm{d}^2F}{\mathrm{d}V^2}\right|_{V=V_0}; \quad F_V^{(3)} = \left.\frac{\mathrm{d}^3F}{\mathrm{d}V^3}\right|_{V=V_0}.$$

Thus, Eq. (3) can be rewritten as

$$M\ddot{x}(t) + kx(t) + F_V^{(1)}\dot{x}(t) - \frac{F_V^{(2)}}{2}\dot{x}^2(t) + \frac{F_V^{(3)}}{6}\dot{x}^3(t) = 0. \tag{5}$$

The non-dimensional form of the above equation is

$$u''(\tau) + u(\tau) + \alpha u'(\tau) - \beta u'^2(\tau) + \gamma u'^3(\tau) = 0, \tag{6}$$

where the prime denotes differentiation with respect to τ and

$$\begin{gathered} \omega = \sqrt{\frac{k}{M}}; \quad \tau = \omega t; \quad x_0 = F(V_0)/k; \\ u(\tau) = \frac{x(\tau)}{x_0}; \quad u'(\tau) = \frac{\mathrm{d}u(\tau)}{\mathrm{d}\tau}; \quad u''(\tau) = \frac{\mathrm{d}^2u(\tau)}{\mathrm{d}\tau^2}; \\ \alpha = \frac{F_V^{(1)}}{\sqrt{Mk}}; \quad \beta = \frac{F_V^{(2)}}{2Mk}F(V_0); \quad \gamma = \frac{F_V^{(3)}}{6(Mk)^{3/2}}F^2(V_0). \end{gathered}$$

2.2. Limit cycle

Eq. (6) can be represented as

$$u''(\tau) + u(\tau) + \varepsilon h(u(\tau)) = 0, \tag{7}$$

where

$$\varepsilon h(u(\tau)) = \alpha u'(\tau) - \beta u'^2(\tau) + \gamma u'^3(\tau).$$

In order to apply an averaging method for solving, the standard Van-der-Pol transformation based on the harmonic solution to the unperturbed problem [20,21] can be used as

$$\begin{aligned} u(\tau) &= A_1(\tau)\sin(\psi(\tau)); \\ u'(\tau) &= A_1(\tau)\cos(\psi(\tau)). \end{aligned} \tag{8}$$

This results in

$$A_1'(\tau) = -\varepsilon h(A_1(\tau)\cos(\psi(\tau)))\cos(\psi(\tau)),$$
$$\psi'(\tau) = 1 + \frac{\varepsilon}{A_1(\tau)} h(A_1(\tau)\cos(\psi(\tau)))\sin(\psi(\tau)). \tag{9}$$

Averaging this system with respect to $\psi(\tau)$, we get an equation for the first-order approximation as

$$A_1' = -\frac{1}{2}\varepsilon A_1\left(\alpha + \frac{3}{4}\gamma A_1^2\right). \tag{10}$$

Now, there are two equilibrium solutions for this equation. $A_1 = 0$ is a trivial solution corresponding to the static equilibrium $u = 0$. The non-trivial solution, which depends on the linear and cubic coefficient, is given by

$$A_1 = \sqrt{-\frac{4\alpha}{3\gamma}}. \tag{11}$$

We have $\alpha < 0$ (negative gradient characteristic of friction force with respect to slip velocity). And a stable periodic solution exists with $\alpha < 0$ and $\gamma > 0$.

3. Experimental setup

For the experimental study of friction-driven oscillations and its control, a setup of friction-driven oscillator with an impact damper has been fabricated as shown in Fig. 2. It consists of a primary mass, which oscillates on a moving belt (1) and a secondary mass (2) freely oscillating on the primary mass between two vertical walls (3), which are fixed to the primary mass. The secondary mass gives impact against these two walls. The primary and secondary masses oscillate along the same line.

The primary mass consists of a mild steel (MS) block (4) of dimensions (40 mm × 35 mm × 25 mm) placed on a rough leather conveyor belt (1). The block is attached to a rigid support through a coiled spring (5) of stiffness equal to 763 N/m. The endless leather conveyor belt moving at a constant speed provides the self-excitation. The belt is held in between two pulleys (6), one of which is driven by a single-phase induction motor (7) with a constant speed of 1440 rpm. The pulley shafts are mounted, with standard bearings, in the cast iron housing (8) placed on very thick and rigid wooden blocks (9). An idler pulley (10) is mounted on slack side of the belt in two brass bushes, which can slide smoothly through a vertical rectangular pipe (11). This vertical adjustment of the idler pulley controls the sag in the belt, which ensures continuous contact between the primary mass and the moving belt.

The oscillation of the primary mass only along the direction of the belt motion is ensured by using a linear motion (LM) bearing. The oscillation in the direction perpendicular to that of the belt motion was found to be almost two orders of magnitude less (and with a much higher frequency). The bearing is fixed on the MS block

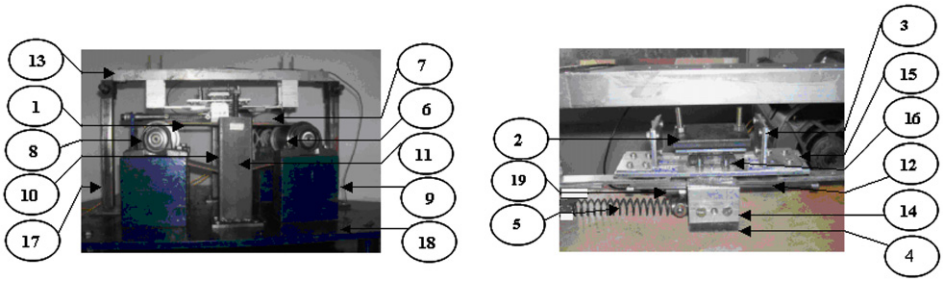

Fig. 2. Experimental setup—(1) leather conveyor-belt; (2) secondary mass; (3) vertical impacting wall; (4) mild steel block; (5) coiled spring; (6) pulley; (7) single-phase induction motor; (8) cast iron housing; (9) wooden block; (10) idler pulley; (11) vertical rectangular pipe; (12) rail of the first LM bearing; (13) rigid aluminum pipe of square c/s; (14) inverted 'L'-shaped Al angle; (15) large rectangular plate with slots; (16) second LM bearing; (17) end stand; (18) heavy base; and (19) accelerometer.

by screws and the rail/slider (12) of LM bearing is fixed to a rigid aluminum pipe (13) of square cross-section, so that the block oscillates along the direction of the rail. Two vertical walls (3) are attached to the primary mass in such a way that the distance between them can be adjusted. This is achieved by leaving a gap for the rail of LM bearing to come out by using two inverted 'L'-shaped aluminum angles (14), which are fixed to the opposite sides of the MS block. One large rectangular aluminum plate (15) of size (150 mm × 40 mm) is fixed on these inverted 'L'-shaped angles. Another two 'L'-shaped aluminum angles are fixed in the slots made on either sides of a large plate (15) by using screws and nuts. The vertical sides of these 'L'-shaped angles act as the vertical impacting walls (3) and the distance between these two walls can be varied using the slots provided on the larger plate. The impacting surfaces of different materials can be fixed to these vertical walls to get different values of the coefficient of restitution. At the center of this large plate, another LM bearing (16) is fixed by screws so that the rail of it is in the direction of the belt movement. Thus, the primary mass consists of the MS block and the whole construction on it described above, including the blocks of the both LM bearings used. The total mass of the primary system is 560 gm including one-third mass effect of the coiled spring attached to the MS block.

One small aluminum plate is fixed on the rail of the second LM bearing (16) and the provision is made to attach the external plates of various masses to this small plate by using screws and nuts. One of these external plates has rounded ends to give a point impact on the vertical impacting surfaces. This assembly acts as a secondary mass and its mass can be altered by changing the external plates attached. Two vertical end stands (17) are used for overall vertical adjustment of this whole assembly of the primary and secondary mass. The whole setup is mounted on a heavy base (18).

The oscillation of the primary system is measured by an accelerometer (19). The output signal from the accelerometer is fed to an FFT analyzer via a charge amplifier. The displacement response and the associated power spectrum are obtained.

4. Determination of friction model parameters

In order to determine the parameter values α, β and γ of the friction model under consideration, a free vibration test is carried out without any damping for $M = 0.56$ kg and $k = 763$ N/m i.e., mass of the secondary mass is equal to zero. It is observed that as soon as the driving motor starts, the primary mass starts to oscillate and attains a steady state generating a limit cycle. The time response curve and the power spectrum obtained experimentally are shown in Figs. 3 and 4, respectively.

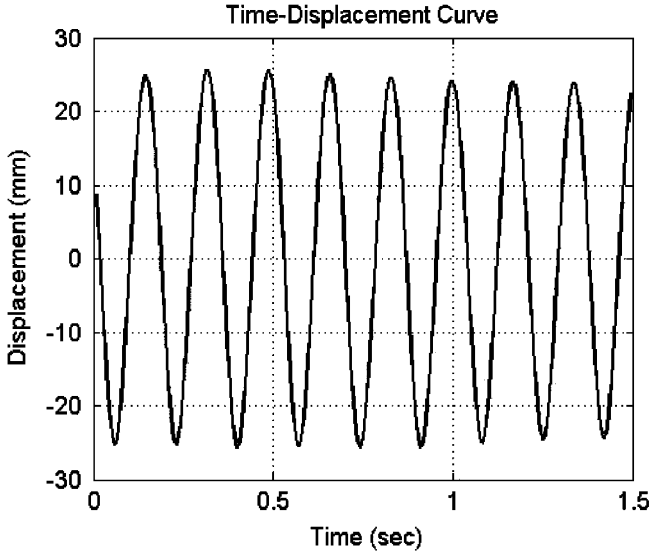

Fig. 3. Time–displacement curve obtained experimentally.

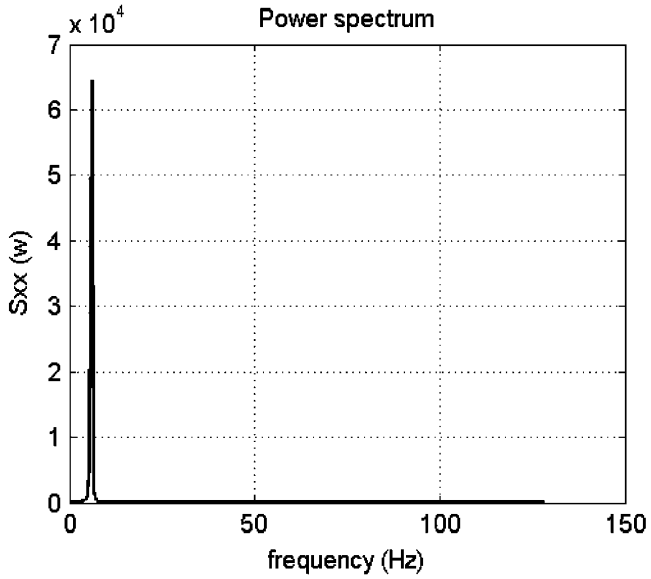

Fig. 4. Power spectrum of the signal.

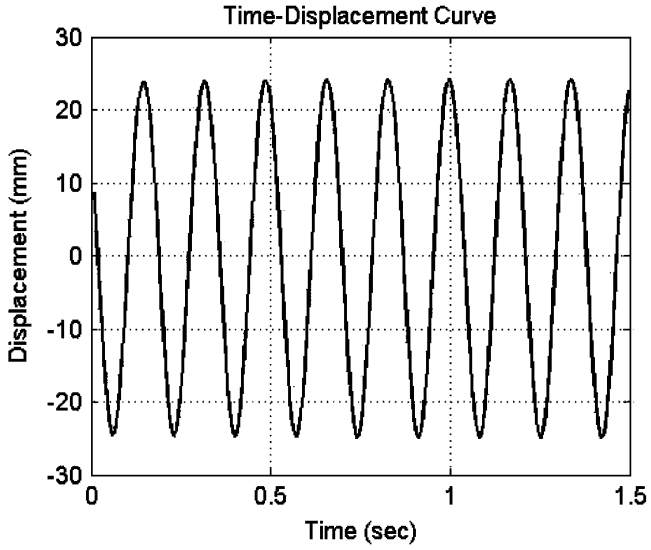

Fig. 5. Time–displacement curve obtained numerically.

It is clearly seen that the displacement response is smooth. Hence, the assumption of pure slip motion is justified. It is also noticed that at the steady state, the primary mass oscillates around a mean position, which is shifted from the static equilibrium position by 10 mm which is equal to the value of $x_0 = F(V_0)/k$.

Numerical simulation of the equation of motion is done to obtain the values of the system parameters α, β and γ to reproduce the above experimental results as closely as possible. In this numerical analysis, a least square error method [22] is used to get these parameters. The backward difference approach [22] is used to get the first- and second-order derivatives of displacement at a point on the time–displacement curve. Towards this end, 4096 points on the experimentally obtained time–displacement curve (for a span of 16 s) are used. The parameter values so obtained [23] are listed below:

$$\alpha = -0.04; \quad \beta = -0.0099; \quad \gamma = 0.0088. \tag{12}$$

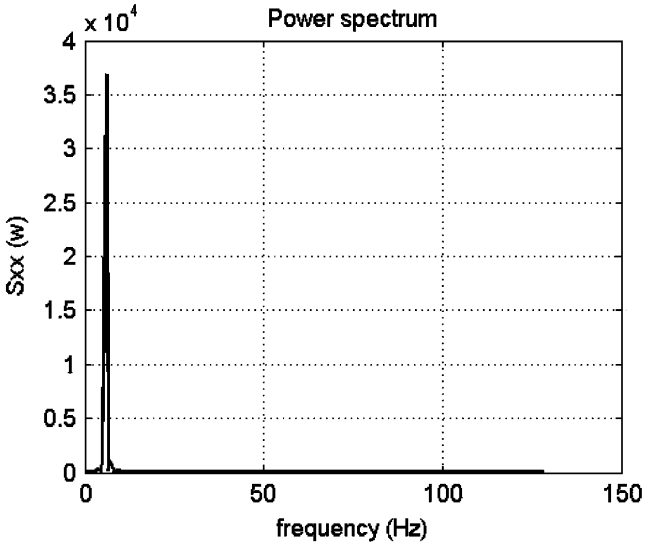

Fig. 6. Power spectrum of the response shown in Fig. 5.

Table 1
shows the experimentally and numerically obtained values of different parameters of the motion of the primary mass

	Experimental	Numerical
Peak–peak displacement	50 mm	49.10 mm
Peak frequency of oscillation	6 Hz	6 Hz
Shift of mean from zero level	−0.30 mm	−0.40 mm

Now, by using the above values, the time–displacement curve and power spectrum obtained numerically are shown in Figs. 5 and 6, respectively (Table 1).

By using Eq. (11), we get $A_1 = 24.671$ mm i.e., the peak-to-peak displacement is 49.342 mm, which is again close to the experimental value. Here and onwards, the values of parameters α, β and γ given in Eq. (12) are used for all analytical and numerical results.

5. Friction-driven oscillator with an impact damper

5.1. Mathematical model

Fig. 7 shows the friction-driven oscillator with an impact damper. Consider the steady-state motion of the system. Here, we derive a periodic solution with two non-symmetric impacts per cycle.

One such cycle is shown in Fig. 8. Without any loss of generality, let us arbitrarily set the time origin $\tau = 0$ at the instant of an impact with the right-hand side wall. Now, the next two consecutive impacts occur at $\tau = \tau_1$ and at $\tau = 2\pi/\Omega$, where Ω is the unknown frequency of the limit cycle. Asymmetric collisions are implied by $\tau \neq \pi/\Omega$. However, for the data used in this work with $\Omega \approx 1$, the difference $|\tau_1 - \pi/\Omega|$ is less than approximately 0.1 signifying a very small amount of asymmetry between the two collisions during a cycle.

The differential equations describing the motion of the system between two consecutive impacts can be written in the following non-dimensional form:

$$\begin{aligned} &x_1''(\tau) + x_1(\tau) + \alpha x_1'(\tau) - \beta x_1'^2(\tau) + \gamma x_1'^3(\tau) = 0, \\ &x_2'' = 0, \text{ or } x_2' = v_1 = \text{constant}, \\ &\quad \ldots \text{ for} |x_1 - x_2| < d_0 \text{ and } 0^+ < \tau < \tau_1^- \end{aligned} \tag{13a}$$

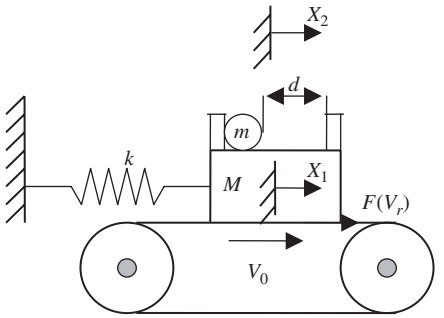

Fig. 7. Mass on a moving belt system with an impact damper.

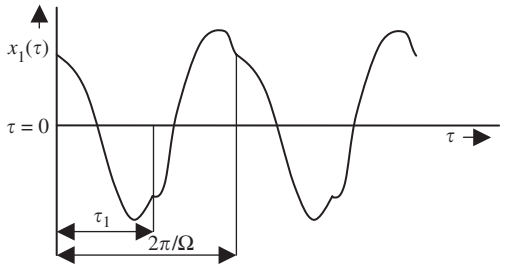

Fig. 8. Two cycles of a typical periodic solution having two non-symmetric impacts per cycle.

and

$$\begin{aligned} &x_1''(\tau) + x_1(\tau) + \alpha x_1'(\tau) - \beta x_1'^2(\tau) + \gamma x_1'^3(\tau) = 0, \\ &x_2'' = 0, \text{ or } x_2' = v_2 = \text{constant}, \\ &\quad \ldots \text{ for} |x_1 - x_2| < d_0 \text{ and } \tau_1^+ < \tau < 2\pi/\Omega^-, \end{aligned} \tag{13b}$$

where

$$\omega = \sqrt{\frac{k}{M}}; \quad \tau = \omega t; \quad x_0 = F(V_0)/k;$$
$$x_1(\tau) = \frac{X_1(\tau) - x_0}{x_0}; \quad x_2(\tau) = \frac{X_2(\tau) - x_0}{x_0}; \quad d_0 = d/2x_0;$$
$$\alpha = \frac{F_V^{(1)}}{\sqrt{Mk}}; \quad \beta = \frac{F_V^{(2)}}{2Mk} F(V_0); \quad \gamma = \frac{F_V^{(3)}}{6(Mk)^{3/2}} F^2(V_0).$$

Impact occurs when $|x_1 - x_2| = d_0$ and the prime denotes differentiation with respect to 'τ'.

5.2. Periodic solution (analytical method)

A piecewise equivalent linearization method [16] is used to obtain the periodic solution of the present system. First we transform Eqs. (13a) and (13b) in the equivalent linear forms as given below:

$$\begin{aligned} &x_1''(\tau) + 2\rho_1 x_1'(\tau) + x_1(\tau) = 0, \\ &. \\ &x_2'' = 0, \textit{ or } x_2' = v_1 = \text{constant}, \\ &\quad \ldots \text{ for} |x_1 - x_2| < d_0 \text{ and } 0^+ < \tau < \tau_1^- \end{aligned} \tag{14a}$$

and

$$x_1''(\tau) + 2\rho_2 x_1'(\tau) + x_1(\tau) = 0,$$
$$\cdot$$
$$x_2'' = 0, \text{ or } x_2' = v_2 = \text{constant},$$
$$\ldots \text{ for} |x_1 - x_2| < d_0 \text{ and } \tau_1^+ < \tau < 2\pi/\Omega^-. \tag{14b}$$

Solving Eqs. (14a) and (14b), one can write the motion between two consecutive impacts for the primary mass as

$$x_1(\tau) = e^{-\rho_1\tau}(c_1 \cos(\omega_{d1}\tau) + d_1 \sin(\omega_{d1}\tau))$$
$$\ldots \text{ for}(0^+ < \tau < \tau_1^-) \tag{15a}$$

and

$$x_1(\tau) = e^{-\rho_2\tau}(c_2 \cos(\omega_{d2}\tau) + d_2 \sin(\omega_{d2}\tau))$$
$$\ldots \text{ for}(\tau_1^+ < \tau < 2\pi/\Omega^-), \tag{15b}$$

where, $\omega_{d1} = \sqrt{1-\rho_1^2}$and $\omega_{d2} = \sqrt{1-\rho_2^2}$.

Here ρ_1 and ρ_2 are unknown constants to be determined. Since there is no force acting on the secondary mass m between impacts, its velocity during the intervals $(0^+ < \tau < \tau_1^-)$ and $(\tau_1^+ < \tau < 2\pi/\Omega^-)$ remains constant and is assumed as v_1 and v_2, in respective intervals.

Now, consider the displacement continuity at the impact as

$$x_1(0^+) = x_1(2\pi/\Omega^-), \tag{16}$$

$$x_1(\tau_1^+) = x_1(\tau_1^-). \tag{17}$$

The definition of the coefficient of restitution (χ) yields

$$\chi = -\frac{\dot{x}_1(0^+) - v_1}{\dot{x}_1(2\pi/\Omega^-) - v_2} \tag{18}$$

when the impact occurs on the right-hand side wall, and

$$\chi = -\frac{\dot{x}_1(\tau_1^+) - v_2}{\dot{x}_1(\tau_1^-) - v_1} \tag{19}$$

when the impact occurs on the left-hand side wall.

Using the conservation of momentum principle, we get

$$M\dot{x}_1(0^+) + mv_1 = M\dot{x}_1(2\pi/\Omega^-) + mv_2 \tag{20}$$

and

$$M\dot{x}_1(\tau_1^+) + mv_2 = M\dot{x}_1(\tau_1^-) + mv_1. \tag{21}$$

From the kinematics of motion of the secondary mass between impacts, we can write

$$x_1(0^+) - x_1(\tau_1^-) + 2d_0 = -v_1\tau_1, \tag{22}$$

$$x_1(2\pi/\Omega^-) - x_1(\tau_1^+) + 2d_0 = v_2(2\pi/\Omega - \tau_1). \tag{23}$$

For determining ρ_1 and ρ_2, let us consider a single-term Fourier series approximation of $x_1(\tau)$ given by

$$x_1^*(\tau) = a\cos(\Omega\tau). \tag{24}$$

Applying the principle of minimizing the average error over the two parts of a cycle for equivalent linearization [16], we get

$$\rho_1 = \frac{\int_0^{\tau_1}\{\alpha x_1^{*\prime 2}(\tau) - \beta x_1^{*\prime 3}(\tau) + \gamma x_1^{*\prime 4}(\tau)\}\mathrm{d}\tau}{2\int_0^{\tau_1}\{x_1^{*\prime 2}(\tau)\}\mathrm{d}\tau}, \tag{25}$$

$$\rho_2 = \frac{\int_{\tau_1}^{2\pi/\Omega_1} \{\alpha x_1^{*'2}(\tau) - \beta x_1^{*'3}(\tau) + \gamma x_1^{*'4}(\tau)\} d\tau}{2\int_{\tau_1}^{2\pi/\Omega} \{x_1^{*'2}(\tau)\} d\tau}. \tag{26}$$

We know that Eqs. (15) and (24) are the two different representations of the same solution. Thus, these two solutions should be equal in some least square sense which implies that the first Fourier component of Eq. (15) should be given as

$$a = \frac{\Omega}{\pi}\left|\int_0^{2\pi/\Omega} x_1(\tau) e^{i\Omega\tau} d\tau\right|. \tag{27}$$

Now, we have total 11 unknowns viz., c_1, d_1, c_2, d_2, ρ_1, ρ_2, v_1, v_2, Ω, τ_1 and a, and 11 nonlinear simultaneous equations. By using these equations we can find out the values of a, Ω and τ_1 (and the other unknowns, if necessary) for known values of α, β, γ, d_0, M, m and χ.

So, the system can be studied analytically to see the effect of the distance d_0 between two impacting walls on the amplitude a of the primary system for the particular values of the coefficient of restitution (χ) and the mass ratio $r_m = m/M$. For solving the above complex system of 11 simultaneous nonlinear equations, eight variables were eliminated algebraically to generate a system of three coupled nonlinear algebraic equations in three variables, viz., a, Ω and τ_1. Thereafter, *fsolve* algorithm in **MATLAB** was used. System behavior is studied for the various values of the coefficient of restitution and mass ratio.

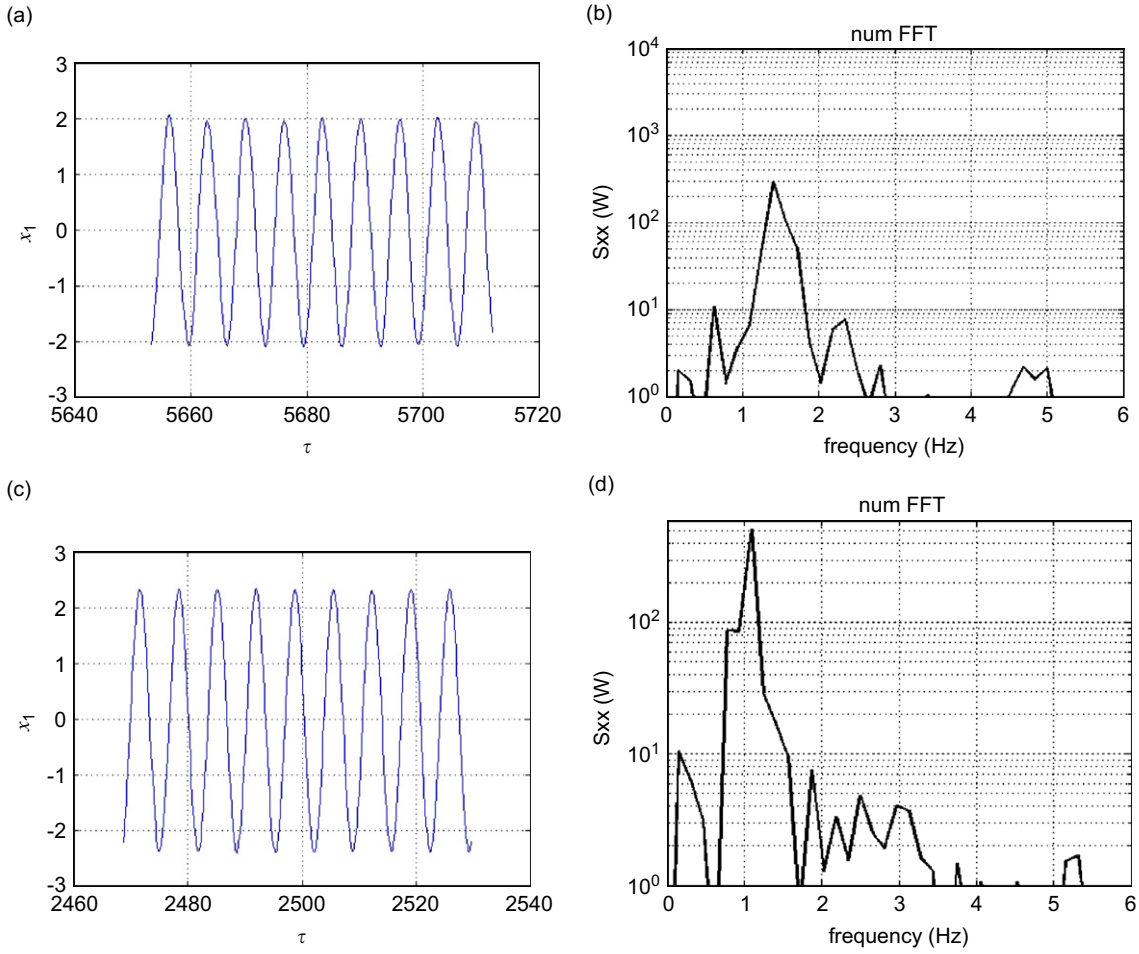

Fig. 9. (a) Times series curve, (b) power spectrum, for, (c) times series curve, (d) power spectrum, for $d_0 = 0.4$ and $r_m = 0.15$.

The system Eqs. (13) are also solved by the numerical method for the same values of the coefficient of restitution and mass ratio. The results are compared with that obtained analytically. For the numerical analysis, Runge–Kutta's integration procedure i.e., **ode45** is used in **MATLAB**.

6. Results and discussion

The system of friction-driven oscillations with an impact damper is solved analytically as well as numerically for the particular range of d_0 where only two impacts occur per cycle. The results are obtained for four different values of the coefficient of restitution $\chi = 0.8$, 0.7, 0.6 and 0.5 and for each value of the coefficient of restitution, four different values of the mass ratio $r_m = 0.08$, 0.10, 0.12 and 0.15 are considered. The solution obtained for the non-dimensional amplitude of the system with damper, defined as controlled amplitude A_c, is compared with the uncontrolled non-dimensional amplitude A_u (i.e., the non-dimensional amplitude without the impact damper).

Experiments have been carried out for steel-on-steel (steel–steel), aluminum-on-aluminum (Al–Al) and aluminum-on-rubber impacts. The values of coefficient of restitution for steel–steel and Al–Al impacts are around 0.7 and 0.6, respectively, with two spherical bodies of the same size and material [19]. As the impacting velocity is less than 1 m/s throughout the experiments, these values have been used for impacts between two surfaces made up of steel or aluminum. All the results are available in Ref. [23]. In what follows, some indicative trends and overall observations are presented.

Figs. 9(a)–(d) show some numerical results for two different values of r_m and d_0 with $\chi = 0.8$. The value of the dominant peak frequency (i.e., Ω) for $d_0 = 1.6$, $r_m = 0.08$ and $\chi = 0.8$ is 0.9484. Higher harmonics are

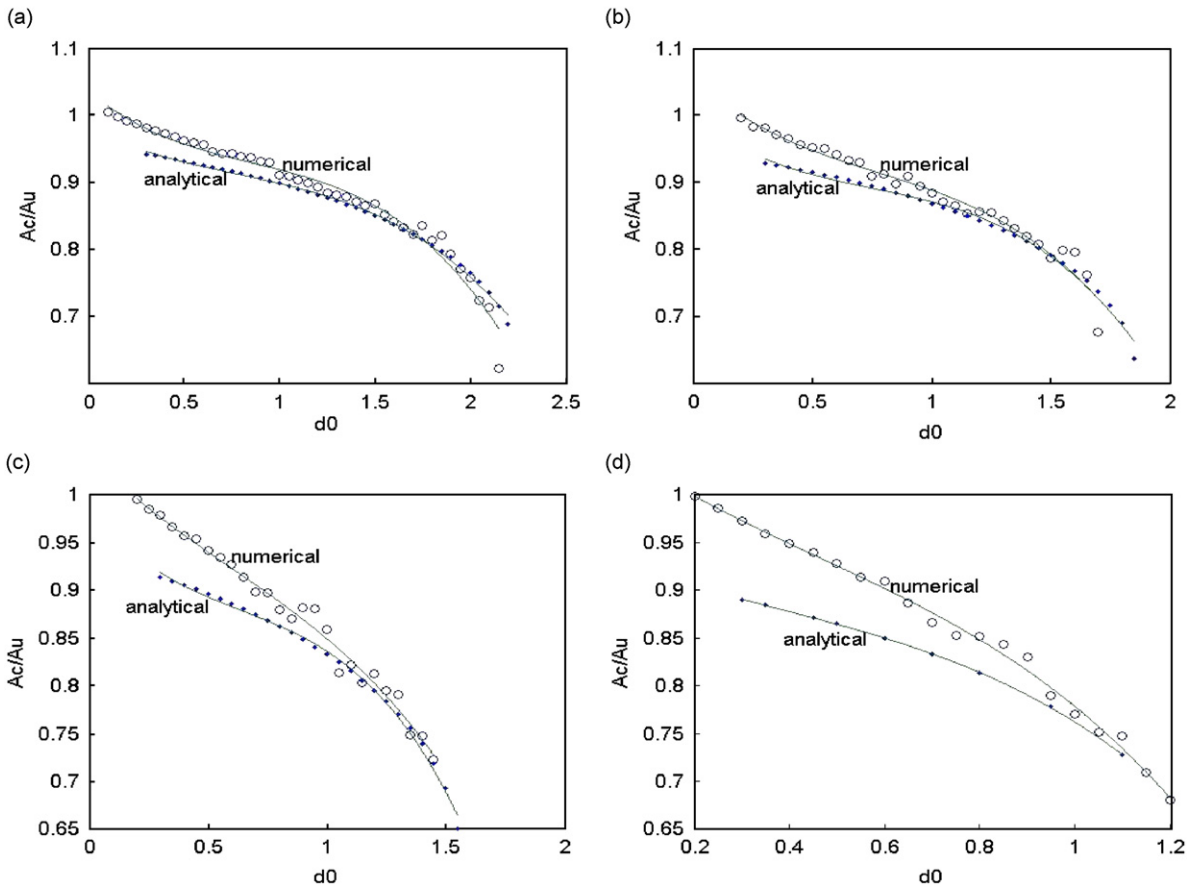

Fig. 10. Numerical and analytical results for $\chi = 0.8$ with (a) $r_m = 0.08$; (b) $r_m = 0.10$; (c) $r_m = 0.12$; and (d) $r_m = 0.15$.

negligible in Fig. 9(b). From Figs. 9(c) and (d), it can be seen that for $d_0 = 0.4$, $r_m = 0.15$ and $\chi = 0.8$, the value of Ω is 0.9308 and very small peaks of the higher harmonics are present indicating that the contribution of higher harmonics increases with increase in mass ratio and decreasing d_0.

In Figs. 10(a)–(d), A_c/A_u is plotted against d_0 for $\chi = 0.8$ and four different values of the mass ratio. Results obtained by both analytical and numerical methods are shown. It is observed that the value of A_c/A_u, i.e., the non-dimensional amplitude of the controlled system, decreases with increasing d_0 and the range of d_0, in which two impacts per cycle occur, decreases with increasing mass ratio.

It is clearly seen that for lower values of r_m and higher values of d_0, analytical and numerical results are quite close. The discrepancy increases with lower values of d_0 and increasing values of r_m. The discrepancy can be attributed to the single-term harmonic approximation in the analytical method. With the increase of the contribution of higher harmonics, the discrepancy also increases.

Figs. 11(a)–(d) show all three solutions, i.e., analytical and numerical results with $\chi = 0.7$ and experimental results for steel–steel impact, for four different values of mass ratio. It is observed that the discrepancy between analytical and numerical results is more than that for $\chi = 0.8$, and increases with lower values of d_0 and increasing values of r_m. Of course, it is known [16] that for lower values of the coefficient of restitution, the equivalent linearization with viscous damping is less accurate. For low values of r_m, the trend exhibited by the experimental results matches with that predicted by the theory. The difference between theoretical and experimental results increases with increasing values of r_m.

From the overall observation of all results (not presented here), it is noticed that the value of the controlled amplitude decreases with higher values of r_m and increasing values of d_0. For lower values

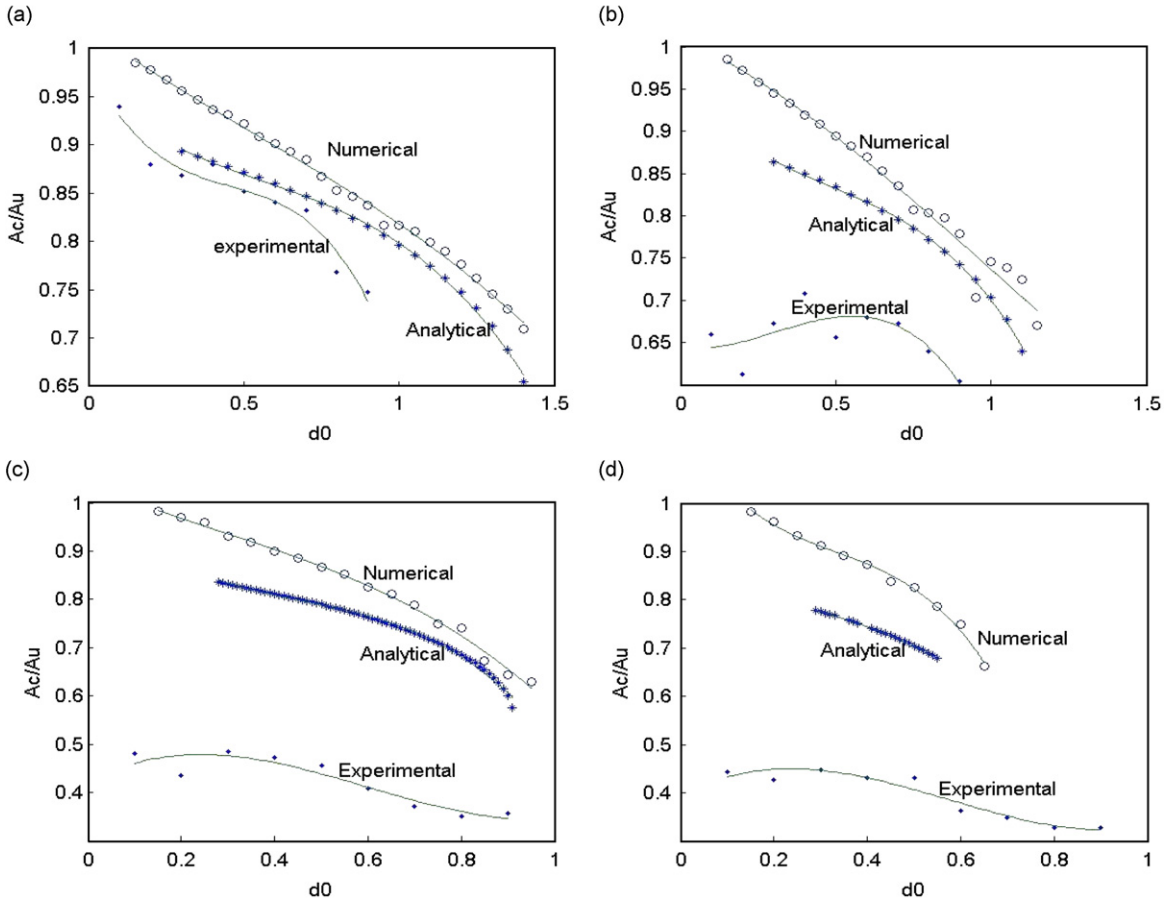

Fig. 11. Numerical and analytical results for $\chi = 0.7$ and experimental results with steel–steel impact for (a) $r_m = 0.08$; (b) $r_m = 0.10$; (c) $r_m = 0.12$; and (d) $r_m = 0.15$.

of r_m, higher values of χ and d_0, the results obtained by all three methods match reasonably well. The discrepancy in these results increases with higher values of r_m, lower values of χ and decreasing values of d_0. It is also seen that the value of A_c/A_u decreases with decreasing values of χ. The primary reason for high discrepancy between theoretical and experimental results is the lack of knowledge about the value of the coefficient of restitution (χ) during the experiment. The results are quite sensitive to the value of χ. Furthermore, the impact damper model is known to have more error for lower values of χ. The contact period between the colliding bodies increases with lower values of χ (towards a plastic collision). So the impact model based on instantaneous transfer of momentum becomes less accurate. The error also increases with a bigger secondary mass, which introduces extra damping and larger contribution to response from the higher harmonics. Neither of these two was accounted for in the theory.

Experimental results obtained for steel–steel, Al–Al and Al-on-rubber impacts are shown in Figs. 12(a)–(d).

It can be clearly seen that the value of A_c/A_u decreases with higher values of r_m and increasing values of d_0. It is also noticed that the Al–Al impact is better for the lower values of r_m (i.e., for 0.08 and 0.10) than the steel–steel impact. But, for the higher values of r_m (i.e., for 0.12 and 0.15), steel–steel impact is better than Al–Al impact. In both the cases, results of aluminum-on-rubber impact lie in between steel–steel and Al–Al impacts. In other words, we can say that at the lower values of mass ratio the dissipation of energy is more effective than the transfer of momentum to the secondary mass, and at the higher values of mass ratio the transfer of momentum is more effective.

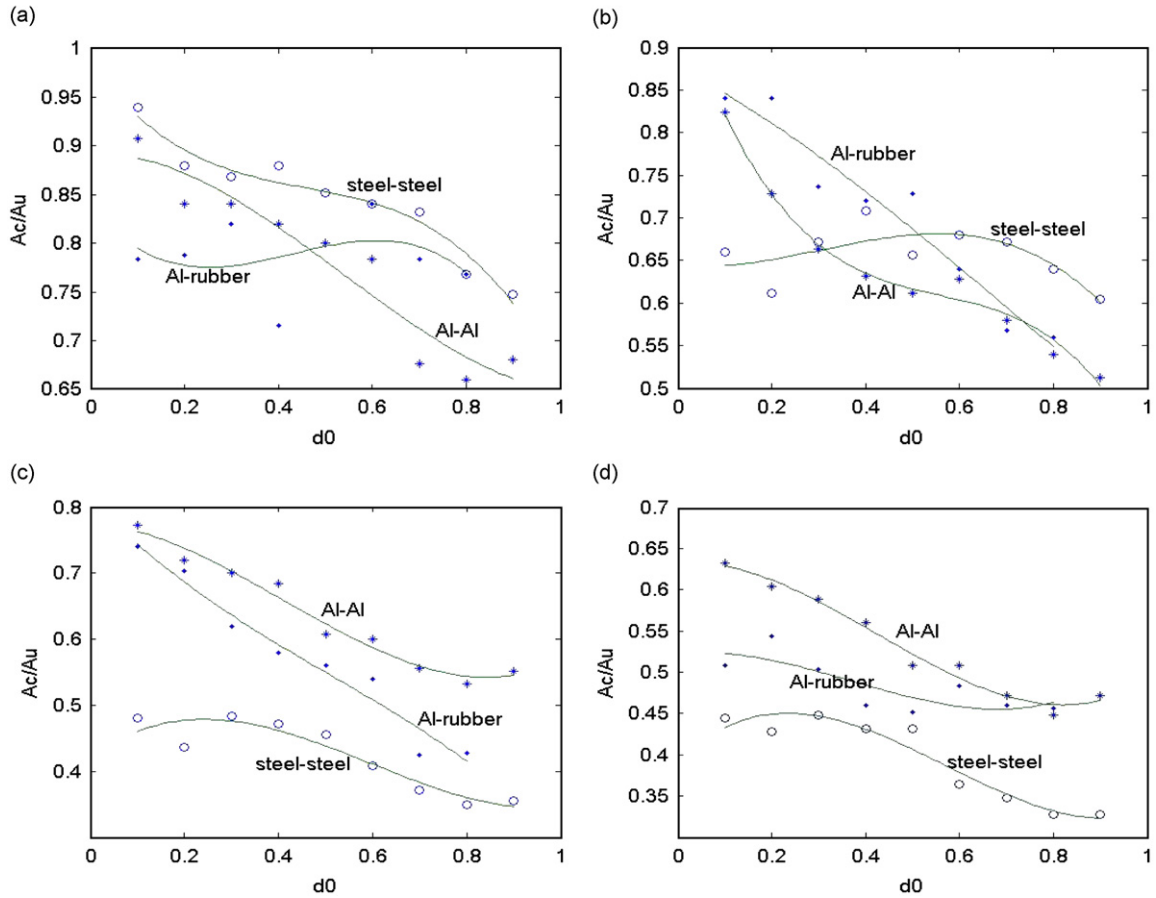

Fig. 12. Experimental results obtained for steel–steel, Al–Al and Al–rubber impacts with (a) $r_m = 0.08$; (b) $r_m = 0.10$; (c) $r_m = 0.12$; and (d) $r_m = 0.15$.

For the lower mass ratio, we do have large span of d_0 to work with and all three solutions i.e., analytical, numerical and experimental results match quite well. Thus, the optimum value of r_m is dictated by the amount of clearance and the material combination.

7. Conclusion

The control of a single degree-of-freedom friction-driven oscillator by using an impact damper is studied analytically, numerically and experimentally. While obtaining a periodic solution for the controlled system by analytical method, it has been observed that when the impact damper undergoes steady-state motion with two impacts per cycle, the amount of asymmetry (depending on the value of β) is negligible. The analytical, numerical and experimental results are pretty close to each other for higher values of the coefficient of restitution, lower values of the mass ratio and increasing values of clearance. But, the discrepancy in these results increases with lower values of clearance, lower values of coefficient of restitution and increasing values of mass ratio. The controlled amplitude of the system decreases with higher values of mass ratio, lower values of the coefficient of restitution and increasing values of clearance. The span of clearance values in which two impacts per cycle occur decreases with higher values of mass ratio and lower values of the coefficient of restitution. The dominant mechanism of vibration control switches from energy dissipation to transfer of momentum with increasing mass ratio.

References

[1] R.A. Ibrahim, Friction-induced vibration, chatter, squeal and chaos. Part I: mechanics of contact and friction, *Applied Mechanics Reviews* 47 (7) (1994) 209–226.
[2] R.A. Ibrahim, Friction-induced vibration, chatter, squeal and chaos. Part II: dynamics and modeling, *Applied Mechanics Reviews* 47 (7) (1994) 227–253.
[3] N. Hinrichs, M. Oestreich, K. Popp, On the modelling of friction oscillators, *Journal of Sound and Vibration* 216 (3) (1998) 435–459.
[4] A. Fidlin, *Nonlinear Oscillations in Mechanical Engineering*, Springer, Berlin, Heidelberg, 2006.
[5] S.L. Qiao, R.A. Ibrahim, Stochastic dynamics of system with friction-induced vibration, *Journal of Sound and Vibration* 223 (1) (1999) 115–140.
[6] J. Das, A.K. Mallik, Control of friction-driven oscillation by time-delayed state feedback, *Journal of Sound and Vibration* 297 (3) (2006) 578–594.
[7] N. Poppelwell, M. Lion, A simple design procedure for optimum impact dampers, *Journal of Sound and Vibration* 146 (3) (1991) 519–526.
[8] A.K. Mallik, *Principles of Vibration Control*, Affiliated East–West Press (P) Ltd., New Delhi, 1990.
[9] C.N. Bapat, S. Sankar, Single unit impact damper in free and forced vibration, *Journal of Sound and Vibration* 99 (1) (1985) 85–94.
[10] B. Blazejczyk-Okolewska, F. Peterka, An investigation of dynamic system with impact, *Chaos, Solitons and Fractals* 9 (1998) 1321–1338.
[11] B. Blazejczyk-Okolewska, Analysis of an impact damper of vibrations, *Chaos, Solitons and Fractals* 12 (2001) 1983–1988.
[12] S. Ema, E. Marui, A fundamental study on impact dampers, *International Journal of Machine Tools and Manufacture* 34 (1994) 407–421.
[13] S. Ema, E. Marui, Damping characteristics of an impact damper and its application, *International Journal of Machine Tools and Manufacture* 36 (1996) 293–306.
[14] S. Ema, E. Marui, Suppression of chatter vibration of boring tool using impact damper, *International Journal of Machine Tools and Manufacture* 40 (2000) 1141–1156.
[15] S. Chatterjee, A.K. Mallik, A. Ghosh, On impact dampers for nonlinear vibrating systems, *Journal of Sound and Vibration* 187 (3) (1995) 403–420.
[16] S. Chatterjee, A.K. Mallik, A. Ghosh, Impact dampers for controlling self excited oscillation, *Journal of Sound and Vibration* 193 (5) (1996) 1003–1014.
[17] S.F. Masri, General motion of impact dampers, *The Journal of Acoustic Society of America* 47 (1970) 229–237.
[18] S.L.T. de Souza, I.L. Caldas, R.L. Viana, J.M. Balthazar, R.M.L.R.F. Brasil, Impact dampers for controlling chaos in systems with limited power supply, *Journal of Sound and Vibration* 279 (2005) 955–967.
[19] W. Goldsmith, *Impact-Theory and Physical Behavior of Colliding Solids*, Edward Arnold (Publishers) Ltd., London, 1960.
[20] A.H. Nayfeh, D.T. Mook, *Nonlinear Oscillations*, Wiley, New York, 1979.
[21] D.W. Jordan, P. Smith, *Nonlinear Ordinary Differential Equations*, Oxford University Press, New York, 1999.
[22] E. Kreszig, *Advanced Engineering Mathematics*, Wiley, New York, 2004.
[23] P.B. Zinjade, Impact Damper for Controlling Friction-Driven Oscillations, MTech Thesis, IIT Kanpur, India, 2006.